

Pericytes regulate the blood–brain barrier

Annika Armulik¹, Guillem Genové¹, Maarja Mäe¹, Maya H. Nisancioglu¹, Elisabet Wallgard^{1†}, Colin Niaudet¹, Liqun He^{1†}, Jenny Norlin¹, Per Lindblom², Karin Strittmatter^{1†}, Bengt R. Johansson³ & Christer Betsholtz¹

The blood–brain barrier (BBB) consists of specific physical barriers, enzymes and transporters, which together maintain the necessary extracellular environment of the central nervous system (CNS)¹. The main physical barrier is found in the CNS endothelial cell, and depends on continuous complexes of tight junctions combined with reduced vesicular transport². Other possible constituents of the BBB include extracellular matrix, astrocytes and pericytes³, but the relative contribution of these different components to the BBB remains largely unknown^{1,3}. Here we demonstrate a direct role of pericytes at the BBB *in vivo*. Using a set of adult viable pericyte-deficient mouse mutants we show that pericyte deficiency increases the permeability of the BBB to water and a range of low-molecular-mass and high-molecular-mass tracers. The increased permeability occurs by endothelial transcytosis, a process that is rapidly arrested by the drug imatinib. Furthermore, we show that pericytes function at the BBB in at least two ways: by regulating BBB-specific gene expression patterns in endothelial cells, and by inducing polarization of astrocyte end-feet surrounding CNS blood vessels. Our results indicate a novel and critical role for pericytes in the integration of endothelial and astrocyte functions at the neurovascular unit, and in the regulation of the BBB.

Platelet-derived growth factor (PDGF)-B/PDGF receptor- β (PDGFR- β) signalling is necessary for pericyte recruitment during angiogenesis^{4,5}. Perinatal lethality precludes analysis of postnatal processes in *Pdgfb* or *Pdgfrb* null mice^{6,7}, but several other mouse mutants of this pathway are viable postnatally. Two such mutants were used here: PDGF-B retention motif knockouts (*Pdgfb*^{ret/ret}) where PDGF-B binding to heparan sulphate proteoglycans was disrupted⁸; and mutants in which *Pdgfb* null alleles were complemented by one or two copies of a conditionally silent human PDGF-B transgene targeted to the *Rosa26* locus and activated by endothelial Cre recombinase (hemizygous R26P^{+/-} or homozygous R26P^{+/+} mice; Supplementary Fig. 2a–d).

We quantified pericyte coverage in different regions of the CNS by CD13 or PDGFR- β staining (Fig. 1a, b, e and Supplementary Fig. 3). *Pdgfb*^{ret/ret}, R26P^{+/-} and R26P^{+/+} mice displayed pericyte coverage corresponding to 26%, 40% and 72%, respectively, compared to controls (Fig. 1a, b). Quantification of absolute numbers of mural cells (pericytes and vascular smooth muscle cells) using the transgenic reporter XLacZ⁹ confirmed low mural cell densities in *Pdgfb*^{ret/ret} and R26P^{+/-} mice, and close to normal levels in R26P^{+/+} mice (Supplementary Fig. 3b–p). We extended previous observations^{4,5,10,11} that reduced pericyte densities correlate with increased vessel diameter and reduced vessel density (Fig. 1c–e and Supplementary Fig. 4). Importantly, these phenotypes were almost completely normalized in R26P^{+/-} mice (Fig. 1d, e and Supplementary Fig. 4a–c).

Increased water content in brains of *Pdgfb*^{ret/ret} mice (Fig. 1f) indicated impairment of the BBB. We tested the BBB integrity in the different mutants using a panel of tracers (Supplementary Table 1). The azo dye Evans blue¹² accumulated in mutant brain parenchyma in a time-dependent fashion (Fig. 1i) and in correlation with pericyte density: it was largest in *Pdgfb*^{ret/ret} mice followed by R26P^{+/-} and R26P^{+/+}

(Fig. 1g, h, j and Supplementary Fig. 5a–c). Similarly, the fluorescent dye cadaverine Alexa Fluor-555 accumulated significantly in the brain parenchyma of *Pdgfb*^{ret/ret} and R26P^{+/-} mice (Fig. 1j and Supplementary Fig. 5d, h, i). Additionally, fluorescently labelled albumin, 70 kDa dextran and IgG passed the BBB in *Pdgfb*^{ret/ret} and R26P^{+/-} mice, but not in controls or in R26P^{+/+} mice (Fig. 1j and Supplementary Fig. 5e–g). These experiments establish a close correlation between pericyte density and permeability across the BBB for a range of tracers of different molecular masses (Supplementary Table 1).

Permeability in CNS vessels is impeded by continuous complexes of endothelial junctions^{13,14}. We studied such complexes in adult pericyte-deficient mutants using markers for adherens (VE-cadherin) and tight (ZO-1 and claudin 5) junctions. *Pdgfb*^{ret/ret}, R26P^{+/-} and controls showed junctional marker expression at similar levels as judged by immunostaining and western blotting (Supplementary Fig. 6a–c and data not shown). The junctional markers were distributed in a pattern consistent with continuous junction complexes in both mutants and controls; however, mutants displayed focally increased junctional width and undulation. These patterns were confirmed by transmission electron microscopy, which failed to reveal any apparent abnormalities in the ultrastructure of endothelial junctions, with the exception that longer and irregular stretches of endothelial overlap were commonly found in pericyte-deficient mutants (Fig. 2c and Supplementary Fig. 6e).

Because continuity, ultrastructure and marker expression were consistent with retained integrity of endothelial junctions in the absence of pericytes, we took advantage of the fixable nature of the fluorescent tracers to explore the route of extravasation in *Pdgfb*^{ret/ret} and R26P^{+/-} mice in more detail. Cadaverine Alexa Fluor-555 accumulated in endothelial cells and in the brain parenchyma in *Pdgfb*^{ret/ret} and R26P^{+/-} mice, but not in controls or in R26P^{+/+} mice (Fig. 2a). Extravasated cadaverine Alexa Fluor-555 localized mainly to neurons (Figs 2a and 3d and Supplementary Fig. 7a). Similar patterns of distribution were observed for fluorescent albumin, IgG and 70 kDa dextran (Fig. 2b and Supplementary Fig. 7b). We also studied the distribution of horseradish peroxidase (HRP, 44 kDa) by transmission electron microscopy. We found increased uptake of HRP specifically in macrovesicular structures in the endothelium in *Pdgfb*^{ret/ret} mice in comparison with controls (Fig. 2c, d and Supplementary Fig. 6d, e). *Pdgfb*^{ret/ret} microvessels also showed marked accumulation of HRP reactivity at the vascular basement membrane, without apparent colocalization with endothelial junctions (Fig. 2c, d and Supplementary Fig. 6d, e). Together, these observations indicate that macromolecular permeability across the BBB in pericyte-deficient vessels occurs through a transcytosis route. Pericyte deficiency was not associated with changes in the polarization or with signs of fenestration in the endothelial cells (Supplementary Figs 4d, 6d, e and 7c), features that characterize the BBB defects observed as a result of impaired Wnt/ β -catenin signalling^{15,16}.

The BBB breaks open in conjunction with stroke, leading to life-threatening CNS oedema. A recent study demonstrated that the tyrosine kinase inhibitor imatinib counteracts oedema in experimental

¹Department of Medical Biochemistry and Biophysics, Division of Vascular Biology, Karolinska Institute, Scheeles väg 2, SE-171 77 Stockholm, Sweden. ²AstraZeneca AB, Clinical Development, SE-431 83 Mölndal, Sweden. ³The Electron Microscopy Unit, Institute for Biomedicine, The Sahlgrenska Academy, University of Gothenburg, PO Box 420, SE-405 30 Gothenburg, Sweden. †Present addresses: Department of Genetics and Pathology, Rudbeck Laboratory, Dag Hammarskjölds väg 20, Uppsala University, SE-751 85 Uppsala, Sweden (E.W.); Applied Biosystems Sweden, Lindhagensgatan 76, PO Box 12650, SE-112 92 Stockholm, Sweden (L.H.); German Cancer Research Center DKFZ, Im Neuenheimer Feld 280, 69120 Heidelberg, Germany (K.S.).

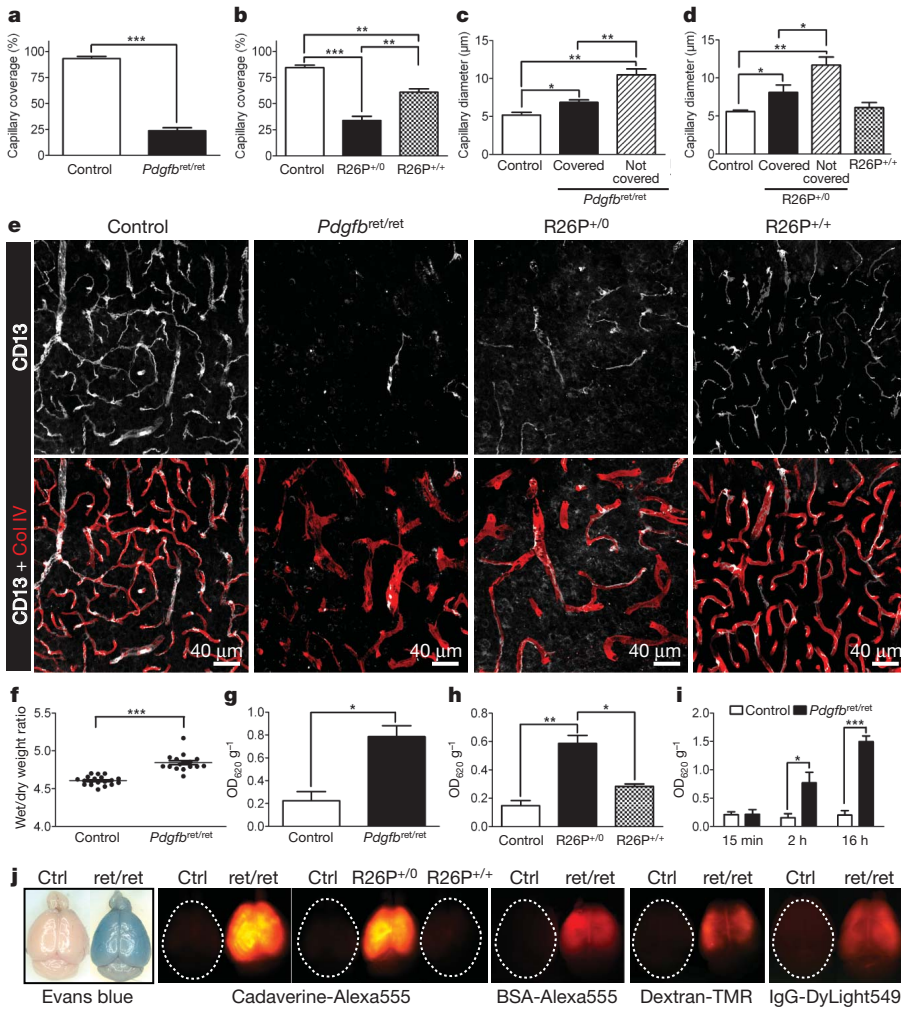


Figure 1 | Pericyte coverage correlates with BBB integrity. **a, b**, Quantification of pericyte coverage of capillaries in the cerebral neocortex of adult *Pdgfb^{ret/ret}* mice (**a**), and *R26P^{+/-}* and *R26P^{+/+}* mice (**b**). **c, d**, Capillary diameter in the cerebral neocortex of adult *Pdgfb^{ret/ret}* mice (**c**), and *R26P^{+/-}* and *R26P^{+/+}* mice (**d**), with or without pericyte coverage. **e**, Three-dimensional reconstructions of confocal image z-stacks of adult cerebral neocortex vasculature depicted by collagen IV (basement membrane) and CD13 (pericyte) staining in *Pdgfb^{ret/ret}*, *R26P^{+/-}* and *R26P^{+/+}* mice. **f**, Wet/dry weight ratios of control and *Pdgfb^{ret/ret}* mice. **g, h**, Quantification of Evans blue in *Pdgfb^{ret/ret}* mice (**g**) and *R26P^{+/-}* and *R26P^{+/+}* mice (**h**) in the cerebrum after 16 h of circulation. **i**, Time course of Evans blue accumulation in the cerebrum of *Pdgfb^{ret/ret}* animals. *y*-axis shows optical density (OD) at 620 nm per gram of tissue. **j**, Whole brains photographed after tracer circulation. Circulation time was 16 h for Evans blue, BSA-Alexa Fluor-555, dextran-TMR and IgG-DyLight 549, and 2 h for cadaverine Alexa Fluor-555. **P* < 0.03; ***P* < 0.007; ****P* < 0.0005. All error bars show mean ± s.e.m.

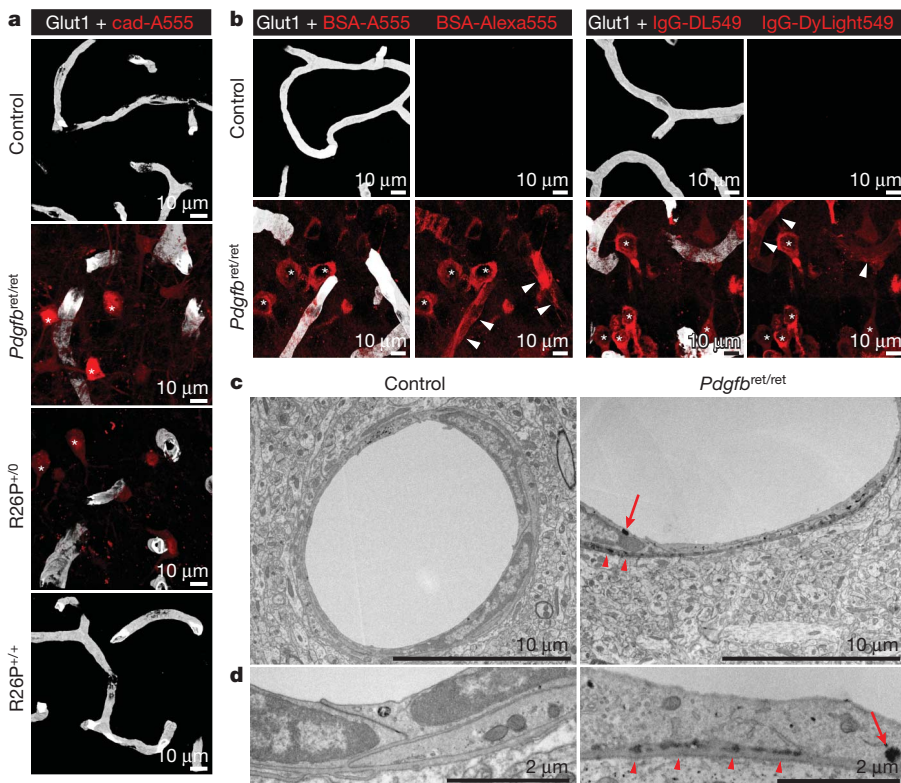


Figure 2 | Pericyte-deficient mice show accumulation of intravenously injected tracers in the brain parenchyma and in the endothelium. **a**, Accumulation of cadaverine Alexa Fluor-555 (red) in the cerebral neocortex in *Pdgfb^{ret/ret}* or *R26P^{+/-}* mice but not in control and *R26P^{+/+}* mice. **b**, Extravasation of BSA-Alexa Fluor-555 (red) and IgG-DyLight 549 (red) in *Pdgfb^{ret/ret}* mice but not in controls. Asterisks in **a** and **b** mark neuronal nuclei. Arrowheads in **b** point to tracer in endothelial cells. Endothelial cells in **a** and **b** are visualized by Glut1 immunostaining (white). **c, d**, Electron microscopy images show HRP in large vesicles (arrows) and at the basal lamina (arrowheads) in *Pdgfb^{ret/ret}* mice.

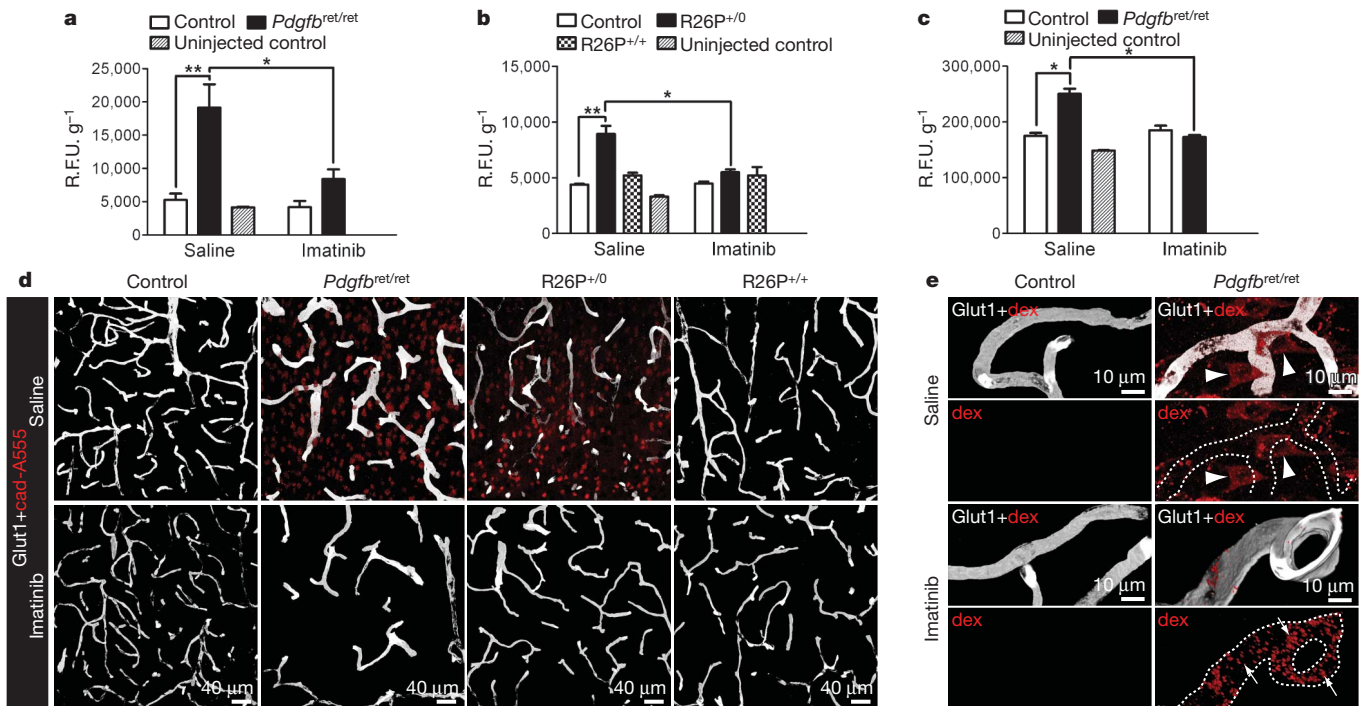


Figure 3 | Imatinib treatment abolishes accumulation of intravenously injected tracers in the brain parenchyma in pericyte-deficient mutants. **a–c**, Quantification of cadaverine Alexa Fluor-555 in *Pdgfb^{ret/ret}* mice (**a**) and *R26P^{+/-}* and *R26P^{+/+}* mice (**b**) in the cerebrum after 2 h of circulation, and of IgG-DyLight 549 (**c**) in *Pdgfb^{ret/ret}* mice in the cerebrum after 16 h of circulation, with and without previous imatinib treatment. *y* axis shows relative fluorescence units (R.F.U.) per gram of tissue. **d, e**, Three-dimensional

reconstructions of confocal image *z*-stacks of cerebral neocortex of mice injected intravenously with cadaverine Alexa Fluor-555 (**d**) or 70 kDa dextran-TMR (**e**). Whereas imatinib abolishes tracer accumulation in neurons in *Pdgfb^{ret/ret}* and *R26P^{+/-}* mice (**d** and arrowheads in **e**), it increases punctuate accumulations in endothelial cells (arrows in **e**). **P* < 0.03; ***P* < 0.005. All error bars show mean ± s.e.m.

stroke induced in mice¹⁷. We found that imatinib treatment quickly and dose-dependently reversed brain parenchymal accumulation of all tested tracers in pericyte-deficient mice (Fig. 3 and Supplementary Fig. 8). In contrast, accumulation and punctuate distribution of fluorescent dextran and IgG in the endothelial cells was enhanced (Fig. 3e and Supplementary Fig. 8b, d, e). This indicates that imatinib inhibits the release of tracer from endothelial cells into the brain parenchyma, consistent with an effect on a late step in the endothelial transcytosis process. Notably, imatinib treatment did not normalize pericyte abundance, vessel diameter, density, or the convoluted appearance of endothelial junctions (Fig. 3d and Supplementary Fig. 9).

To address whether pericytes regulate brain-specific endothelial differentiation we used microarrays to assess the expression of known BBB markers³ in microvascular fragments isolated from adult pericyte-deficient mutants and controls. Such fragments mostly consist of endothelial cells¹⁸, but also include pericytes (when present) and astrocyte end-feet. We used previously obtained array data on embryonic brain microvascular fragments, isolated kidney glomeruli and whole brain for comparison^{18–20}. These analyses show that most BBB markers are unaffected by pericyte deficiency at the mRNA level (Fig. 4a, b and Supplementary Table 2). Two known BBB markers for which antibodies were available were assessed at the level of protein expression: Glut1 (predicted to be unaffected by pericyte deficiency) and transferrin receptor (CD71) (predicted to be downregulated in the pericyte-deficient state). In agreement with the gene expression data, we found that Glut1 protein was uniformly expressed in brain endothelial cells irrespective of the degree of pericyte coverage (Figs 2–4 and Supplementary Fig. 10), whereas CD71 expression was downregulated in the endothelium lacking pericyte contact (Supplementary Fig. 10). Together, these results indicate that pericytes exert a discrete influence on the endothelial BBB-specific gene and protein expression profile.

Astrocytes attach to blood vessels through cap-like cytoplasmic processes—end-feet—carrying specific channels and transporters,

for example, aquaporin 4 (Aqp4) and Kir4.1, which are targeted to astrocyte end-feet to control water and ion homeostasis at the vessel–neuron interface³. Little is known about how contacts between blood vessels and astrocyte end-feet are established and maintained²¹. Our gene array data indicated downregulation of several astrocyte markers in pericyte-deficient brain microvascular fragments (Supplementary Table 2 and data not shown). We therefore asked if pericytes, which are partially sandwiched between the endothelial cells and the astrocyte end-feet, might affect astrocytes, and, specifically, if pericyte deficiency leads to changes in astrocyte end-foot distribution or polarization. Three markers for the polarized astrocyte end-foot, Aqp4, α -syntrophin and laminin α 2 chain (Lama2), all provided uniform labelling of microvessel abluminal surfaces in control brains, consistent with a polarized expression of these markers (Fig. 4c–e and Supplementary Fig. 11). However, in pericyte-deficient mutants, the vascular staining for these markers was weaker than in controls, and the Aqp4 staining was also re-distributed to other regions of the astrocytes, indicating abnormal polarization of the astrocyte end-feet (Supplementary Fig. 11). Interestingly, we found that pericytes that were detached from the endothelial cells showed intense lining with Aqp4 and α -syntrophin immunostaining (Fig. 4d and data not shown). This indicates that pericytes express cues that mediate attachment of astrocyte end-feet. The strong reduction in deposition of the astrocyte-derived basement membrane component Lama2 (Fig. 4e) prompted us to study the expression of a range of other vascular basement membrane components. These analyses failed to show any significant changes in the deposition of endothelium-derived basement membrane proteins laminin α 4, laminin α 5, nidogen and perlecan in pericyte-deficient vessels (Supplementary Fig. 12).

BBB properties are not intrinsic to CNS endothelial cells, but are induced when the cells are in contact with astrocytes *in vitro* and *in vivo*^{22–24}. Recent evidence also suggests a role for neuronal precursors and Wnt signalling in BBB induction *in vivo*^{15,16,25}. A role for pericytes

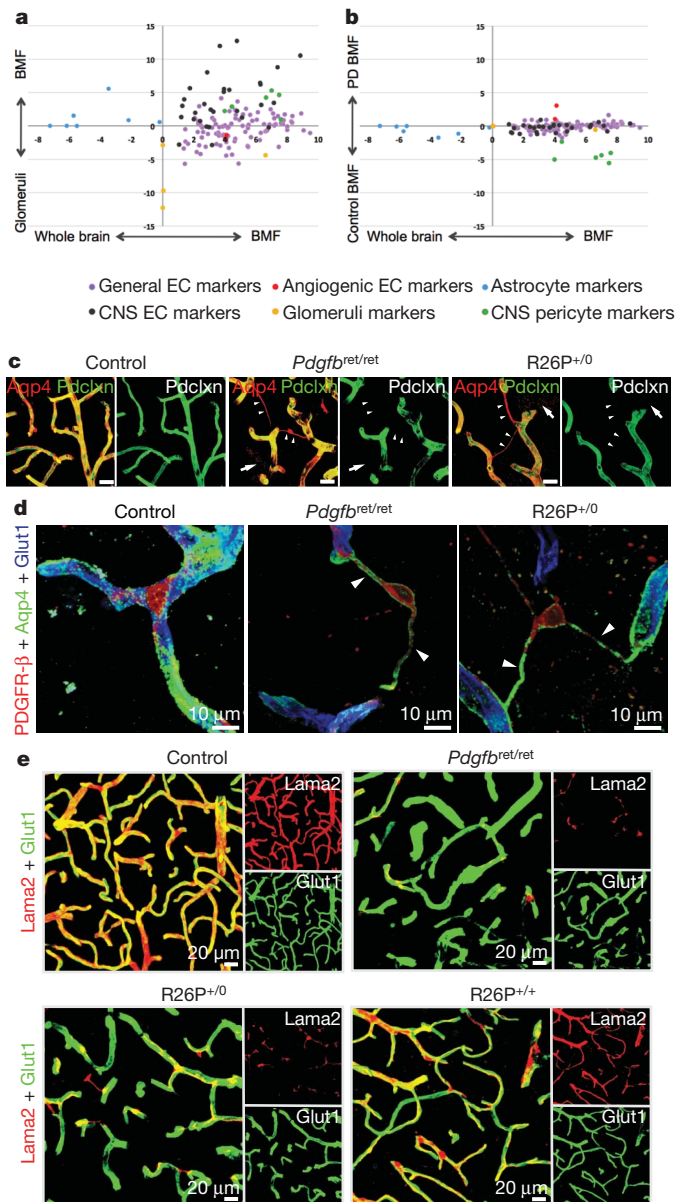


Figure 4 | Transcript profiling of brain microvasculature and characterization of the polarization defect of astrocyte end-feet in pericyte-deficient mutants. **a**, Relative expression (\log_2 fold difference) of known markers for the BBB, endothelial cells, astrocytes, pericytes and glomerular podocytes in adult brain microvascular fragments (BMF) versus whole brain (x axis) and brain microvascular fragments versus glomeruli (y axis). Note the higher expression of BBB markers in brain microvascular fragments compared to glomeruli. **b**, Relative expression of the same genes as in **a** for control and pericyte-deficient (PD) mutants (y axis; see Supplementary Tables 2 and 3 for gene identifiers and further information on methodology). **c**, **d**, Astrocyte end-feet (red) localize to microvessels (green) in controls but also to structures bridging adjacent vessels in *Pdgfn*^{ret/ret} and R26P^{+/-} mice (arrowheads in **c**) that were identified as detached PDGFR- β positive pericytes (**d**, arrowheads). Arrows in **c** point to diffuse Aqp4 staining (red) in pericyte-deficient mice not associated with vessels (see also Supplementary Fig. 11a). Pdgfn, podocalyxin. **e**, *Pdgfn*^{ret/ret} and R26P^{+/-} have reduced deposition of the astrocyte-derived basement membrane component laminin $\alpha 2$ -chain compared to control and R26P^{+/-} animals. Scale bars in **c**, 20 μm .

in endothelial barrier formation has been suggested based on *in vitro* co-culture experiments^{26,27}, but evidence for any specific role of pericytes in BBB formation has so far been lacking. Here we provide evidence for an *in vivo* role of pericytes in regulating the mammalian BBB (schematically illustrated in Supplementary Fig. 1). The increased

endothelial transcytosis that occurs as a result of brain pericyte deficiency in the mouse mutants is compatible with a normal lifespan of the mouse mutants, in spite of the fact that this increase results in oedema and extravasation of plasma proteins in the brain. This is probably tolerated because leakage is slow, allowing the brain to adapt and compensate for any resulting changes in the interstitial environment. Viable pericyte-deficient animal models should therefore be useful in further studies of the putative functional consequences of BBB impairments for higher and integrated neuronal functions, learning and behaviour, and for the progression of brain diseases. Notably, we have demonstrated that the pericyte-deficient state makes the BBB permeable to immunoglobulins. Further elucidation of the molecular mechanisms that trigger opening and closure of this route across the BBB should therefore be of pharmaceutical significance.

METHODS SUMMARY

Animals. The following transgenic mouse lines were used for experiments: PDGF-B knockout⁶, PDGF-B retention motif knockout⁸, Tie2Cre (ref. 28), Rosa26 hPDGF-B (this study), XLacZ (ref. 9) and Z/EG (ref. 29). Animal experiments were approved by the Stockholm's North Ethical Committee for Animal Research. **Generation of Rosa26 hPDGF-B mice.** A full-length human PDGF-B cDNA sequence preceded by a splice acceptor site and a loxP-site-flanked transcription stop cassette was cloned into a vector designed for homologous recombination into the ubiquitously expressed ROSA26 locus³⁰ (Supplementary Fig. 2a). Gene-targeted mice were generated from the ES cells by standard methods. A detailed description is provided in Methods.

Intravenous injection of tracers and detection of injected tracers. The following tracers were used: Evans blue (Sigma Aldrich), lysine-fixable cadaverine conjugated to Alexa Fluor-555 (Invitrogen), bovine serum albumin conjugated to Alexa Fluor-555 (Invitrogen), lysine-fixable 70 kDa dextran conjugated to tetramethylrhodamine (TMR) (Invitrogen), and goat anti-human IgG conjugated to DyLight 549 (Jackson ImmunoResearch Laboratories). Evans blue in the brain was quantified by spectrophotometry as described¹⁷. Detailed information about the quantification of cadaverine-Alexa Fluor-555 and DyLight-549 conjugated goat anti-human IgG in the brain is given in Methods. When indicated, animals were treated with three or four doses of imatinib (150 mg kg⁻¹) twice per day before tracer injections.

Statistical analysis. Statistical significance was determined by using unpaired two-tailed or one-tailed Student's *t*-test (GraphPad Prism5). Differences were considered significant with a *P* value less than 0.05. Quantified data are presented as mean \pm s.e.m.

Full Methods and any associated references are available in the online version of the paper at www.nature.com/nature.

Received 29 April 2009; accepted 23 September 2010.

Published online 13 October 2010.

- Abbott, N. J., Rönnbäck, L. & Hansson, E. Astrocyte-endothelial interactions at the blood-brain barrier. *Nature Rev. Neurosci.* **7**, 41–53 (2006).
- Reese, T. S. & Karnovsky, M. J. Fine structural localization of a blood-brain barrier to exogenous peroxidase. *J. Cell Biol.* **34**, 207–217 (1967).
- Bernacki, J. *et al.* Physiology and pharmacological role of the blood-brain barrier. *Pharmacol. Rep.* **60**, 600–622 (2008).
- Enge, M. *et al.* Endothelium-specific platelet-derived growth factor-B ablation mimics diabetic retinopathy. *EMBO J.* **21**, 4307–4316 (2002).
- Bjarnegård, M. *et al.* Endothelium-specific ablation of PDGFB leads to pericyte loss and glomerular, cardiac and placental abnormalities. *Development* **131**, 1847–1857 (2004).
- Levéen, P. *et al.* Mice deficient for PDGF B show renal, cardiovascular, and hematological abnormalities. *Genes Dev.* **8**, 1875–1887 (1994).
- Soriano, P. Abnormal kidney development and hematological disorders in PDGF β -receptor mutant mice. *Genes Dev.* **8**, 1888–1896 (1994).
- Lindblom, P. *et al.* Endothelial PDGF-B retention is required for proper investment of pericytes in the microvessel wall. *Genes Dev.* **17**, 1835–1840 (2003).
- Tidhar, A. *et al.* A novel transgenic marker for migrating limb muscle precursors and for vascular smooth muscle cells. *Dev. Dyn.* **220**, 60–73 (2001).
- Lindahl, P. *et al.* Pericyte loss and microaneurysm formation in PDGF-B-deficient mice. *Science* **277**, 242–245 (1997).
- Hellström, M. *et al.* Lack of pericytes leads to endothelial hyperplasia and abnormal vascular morphogenesis. *J. Cell Biol.* **153**, 543–554 (2001).
- Moos, T. & Møllgård, K. Cerebrovascular permeability to azo dyes and plasma proteins in rodents of different ages. *Neuropathol. Appl. Neurobiol.* **19**, 120–127 (1993).
- Dejana, E., Tournier-Lasserre, E. & Weinstein, B. M. The control of vascular integrity by endothelial cell junctions: molecular basis and pathological implications. *Dev. Cell* **16**, 209–221 (2009).

14. Taddei, A. *et al.* Endothelial adherens junctions control tight junctions by VE-cadherin-mediated upregulation of claudin-5. *Nature Cell Biol.* **10**, 923–934 (2008).
15. Stenman, J. M. *et al.* Canonical Wnt signaling regulates organ-specific assembly and differentiation of CNS vasculature. *Science* **322**, 1247–1250 (2008).
16. Liebner, S. *et al.* Wnt/beta-catenin signaling controls development of the blood-brain barrier. *J. Cell Biol.* **183**, 409–417 (2008).
17. Su, E. J. *et al.* Activation of PDGF-CC by tissue plasminogen activator impairs blood-brain barrier integrity during ischemic stroke. *Nature Med.* **14**, 731–737 (2008).
18. Bondjers, C. *et al.* Microarray analysis of blood microvessels from PDGF-B and PDGF-R β mutant mice identifies novel markers for brain pericytes. *FASEB J.* **20**, 1703–1705 (2006).
19. Wallgard, E. *et al.* Identification of a core set of 58 gene transcripts with broad and specific expression in the microvasculature. *Arterioscler. Thromb. Vasc. Biol.* **28**, 1469–1476 (2008).
20. He, L. *et al.* The glomerular transcriptome and a predicted protein-protein interaction network. *J. Am. Soc. Nephrol.* **19**, 260–268 (2008).
21. Wolburg, H. *et al.* Agrin, aquaporin-4, and astrocyte polarity as an important feature of the blood-brain barrier. *Neuroscientist* **15**, 180–193 (2009).
22. Janzer, R. C. & Raff, M. C. Astrocytes induce blood-brain barrier properties in endothelial cells. *Nature* **325**, 253–257 (1987).
23. Hayashi, Y. *et al.* Induction of various blood-brain barrier properties in non-neural endothelial cells by close apposition to co-cultured astrocytes. *Glia* **19**, 13–26 (1997).
24. Sobue, K. *et al.* Induction of blood-brain barrier properties in immortalized bovine brain endothelial cells by astrocytic factors. *Neurosci. Res.* **35**, 155–164 (1999).
25. Daneman, R. *et al.* Wnt/ β -catenin signaling is required for CNS, but not non-CNS, angiogenesis. *Proc. Natl Acad. Sci. USA* **106**, 641–646 (2009).
26. Hori, S. *et al.* A pericyte-derived angiopoietin-1 multimeric complex induces occludin gene expression in brain capillary endothelial cells through Tie-2 activation *in vitro*. *J. Neurochem.* **89**, 503–513 (2004).
27. Dohgu, S. *et al.* Brain pericytes contribute to the induction and up-regulation of blood-brain barrier functions through transforming growth factor- β production. *Brain Res.* **1038**, 208–215 (2005).
28. Kisanuki, Y. Y. *et al.* Tie2-Cre transgenic mice: a new model for endothelial cell-lineage analysis *in vivo*. *Dev. Biol.* **230**, 230–242 (2001).
29. Novak, A. *et al.* Z/EG, a double reporter mouse line that expresses enhanced green fluorescent protein upon Cre-mediated excision. *Genesis* **28**, 147–155 (2000).
30. Zambrowicz, B. P. *et al.* Disruption of overlapping transcripts in the ROSA β geo 26 gene trap strain leads to widespread expression of β -galactosidase in mouse embryos and hematopoietic cells. *Proc. Natl Acad. Sci. USA* **94**, 3789–3794 (1997).

Supplementary Information is linked to the online version of the paper at www.nature.com/nature.

Acknowledgements We thank U. Eriksson and members of the Betsholtz laboratory for discussion, P. Soriano, L. Sorokin and R. Hallman for reagents, and S. Kamph and the Scheele animal house for technical assistance. This work was supported by the Leducq Foundation, the Swedish Governmental Agency for Innovation Systems (Vinnova), the EU Fp6 Program Lymphangiogenomics, the Swedish Cancer Society and Research Council, the Knut and Alice Wallenberg, Inga-Britt and Arne Lundberg, and Torsten and Ragnar Söderberg Foundations.

Author Contributions A.A. and C.B. conceived and designed the project. A.A., G.G., M.M., M.H.N., E.W., C.N., L.H., J.N., P.L., K.S. and B.R.J. performed experiments; C.B. and A.A. wrote the manuscript with significant input from M.M., G.G. and M.H.N. G.G. and M.M. contributed equally to the study.

Author Information Our microarray data have been deposited in NCBI's Gene Expression Omnibus (<http://www.ncbi.nlm.nih.gov/geo/>) and are accessible through GEO series accession number GSE15892. Reprints and permissions information is available at www.nature.com/reprints. The authors declare no competing financial interests. Readers are welcome to comment on the online version of this article at www.nature.com/nature. Correspondence and requests for materials should be addressed to C.B. (christer.betsholtz@ki.se) or A.A. (annika.armulik@ki.se).

METHODS

Animals. Progeny from the following transgenic mouse lines were used for experiments: PDGF-B knockout⁶, PDGF-B retention motif knockout⁸, Tie2Cre (ref. 28), Rosa26 hPDGF-B (this study), XLaCZ4 (ref. 9), Z/EG (ref. 29). PDGF-B retention motif knockouts were analysed on a C57BL6/J genetic background and R26P⁺⁰ and R26P^{+/+} animals on a mixed C57BL6/J and 129sv genetic background. Animal experiments were approved by the Stockholm's North Ethical Committee for Animal Research.

Generation of Rosa26 hPDGF-B mice. A DNA cassette consisting of a full-length human PDGF-B cDNA sequence preceded by a splice acceptor site and a loxP-site-flanked transcription stop cassette was cloned into a vector designed for homologous recombination into the ubiquitously expressed ROSA26 locus³⁰ (Supplementary Fig. 2a). The targeting vector was verified by sequencing and electroporated into endothelial cells. Positive clones were identified by PCR and confirmed by Southern blot hybridization as described³⁰. Gene-targeted mice were generated from the ES cells by standard methods. Animal genotyping was done by PCR. The following PCR primers were used: R26F2, 5'-AAAGTCGCTCTGAGTTGTTAT-3'; R26SR, 5'-CCCACTGGAAAGACCGCAAGAGT-3'; R523, 5'-GGAGCGGGAGAAATGGATATG-3' generated a 250-bp PCR fragment from the mutant allele and a 500-bp fragment from the wild-type allele. Expression of hPDGF-B was activated in endothelial cells by crossing with Tie2Cre transgenes (Supplementary Fig. 2b).

Quantification of vessel diameter, density and pericyte coverage. Quantification of vessel pericyte coverage was performed on 50 µm vibratome brain sections. Four corresponding areas in three animals of each genotype were analysed at 3–5 months of age. Blood vessels were visualized by collagen IV and pericytes by CD13 or PDGFR-β immunostainings. 14–16-µm-thick z-stacks were captured using an LSM Meta 510 microscope (Carl Zeiss AG). Quantification of pericyte numbers, vessel length and diameter was performed using Volocity software (Improvision, a PerkinElmer Company).

Antibodies and immunohistochemistry. The following primary antibodies were used: rabbit anti-rat aquaporin 4 (AB3068, Chemicon); rat anti-mouse CD13 (558744, BD PharMingen); rabbit anti-mouse collagen IV (2150-1470, AbD Serotec); rabbit anti-Glut1 (07-1401, Millipore); rat anti-mouse PDGFR-β (14-1402, eBioscience); goat anti-mouse podocalyxin (AF1556, R&D Systems). Secondary antibodies (goat anti-rat, goat anti-rabbit, donkey anti-goat) conjugated with Alexa Fluor dyes were obtained from Invitrogen. For immunostainings in which two primary rabbit antibodies were used, one was directly labelled using the Zenon rabbit IgG labelling kit (Invitrogen). Immunohistochemistry was performed on 50 or 100 µm brain coronal vibratome sections. Specimens were analysed using an LSM 510 META (Carl Zeiss AG) microscope. Image processing was done using Volocity 64 (Improvision), Adobe Photoshop CS3, and Adobe Illustrator CS3 (Adobe Systems). All immunohistochemistry images presented are three-dimensional reconstructions of z-stacks.

Intravenous injection of tracers and detection of injected tracers. Tracers were injected intravenously into the tail vein in adult (2–8 months) mice. The following tracers were used: Evans blue (Sigma Aldrich), lysine-fixable cadaverine conjugated to Alexa Fluor-555 (Invitrogen), bovine serum albumin conjugated to Alexa Fluor-555 (Invitrogen), lysine-fixable 70 kDa dextran conjugated to tetramethylrhodamine (Invitrogen), and goat anti-human IgG conjugated to DyLight 549 (Jackson ImmunoResearch Laboratories). More detailed descriptions of the tracer experiments are given in the Supplementary Methods. Images of dissected brains were captured using a stereomicroscope (SteREO Lumar.V12, equipped with HBO 100 lamp and a Filter Set Lumar 43 HE; Carl Zeiss AG) equipped with an

AxioCam HRc (Carl Zeiss AG) camera. Evans blue in the brain was quantified by spectrophotometry as described¹⁷. For quantification of cadaverine-Alexa Fluor-555 and DyLight-549 conjugated goat anti-human IgG in the brain, anaesthetized animals were perfused for 5 min with Hanks' balanced salt solution (HBSS), brains and kidneys removed and homogenized in 1% Triton X-100 in PBS, pH 7.2. Brain and kidney lysates were centrifuged at 16,000 r.p.m. for 20 min and the relative fluorescence of the supernatant was measured on a fluorometer POLARstar Omega (BMG Labtech) (ex/em 544/590 nm). For *in situ* detection of fluorophore-conjugated tracers, anaesthetized animals were perfused for 1–2 min with HBSS, followed by 5 min perfusion with 4% PFA in PBS, pH 7.2. Brains were removed and the tissue was post-fixed in 4% PFA in PBS, pH 7.2 at 4 °C for 5–6 h. 50-µm-thick coronal brain sections were immunostained with anti-Glut1 antibody. Samples were analysed by confocal microscopy (LSM 510 META, Carl Zeiss AG). When indicated, animals were treated with three or four doses of imatinib (150 mg kg⁻¹) twice per day before tracer injections.

Transmission electron microscopy. Two-month-old mice were injected intravenously with horseradish peroxidase Type II (HRP) (100 mg ml⁻¹ in PBS, 10 mg per 20 g) (Sigma Aldrich). After 2 h, animals were anaesthetized and perfused with 2.5% glutaraldehyde in 0.1 M cacodylate buffer, pH 7.2. HRP-diaminobenzidine cytochemistry was performed on brain vibratome slices according to ref. 31 with minor modifications. After osmication and en bloc uranyl acetate treatment, tissue blocks were dehydrated and embedded in epoxy resin. Sections were cut with a diamond knife on a Leica EM UC7 ultramicrotome (Leica Microsystems) at 60 nm thickness setting and were examined without additional contrasting in a LEO 912AB energy-filtered transmission electron microscope (Carl Zeiss SMT AG). Digital images were captured with a MegaView III camera (Olympus SIS).

Brain water content determination. Animals were anaesthetized and perfused with HBSS for 5 min via the left ventricle of the heart. Brains were removed and weighed for wet weight. Tissue was dried at 62 °C for 6 days and weighed again for dry weight.

Purification of microvasculature and microarray analysis. Purification of microvasculature and RNA isolation was performed as described²⁰. Four RNA samples of each genotype were individually hybridized to Affymetrix GeneChip Mouse Genome 430 2.0 microarrays. Publicly available Affymetrix raw data files concerning wild-type adult whole brain³², isolated wild-type adult glomeruli²⁰, and wild-type embryonic and adult brain microvascular fragments¹⁹ were downloaded and treated in the same manner as data generated in this study. Array data was processed using the Affy and gcrma packages in the Bioconductor project (<http://www.bioconductor.org>). A Student's *t*-test was used to evaluate differential expression. The false discovery rate method was used to perform multiple test correction for *P* values³³. The log₂ change was calculated as the log₂ of the average expression difference between sample groups. A detailed description of the samples used in different comparisons is given in Supplementary Table 3.

Statistical analysis. Statistical significance was determined by using unpaired two-tailed or one-tailed Student's *t*-test (GraphPad Prism5). Differences were considered significant with a *P* value less than 0.05. Quantified data are presented as mean ± s.e.m.

1. Karnovsky, M. J. The ultrastructural basis of capillary permeability studied with peroxidase as a tracer. *J. Cell Biol.* **35**, 213–236 (1967).
2. Bender, A. *et al.* Creatine improves health and survival of mice. *Neurobiol. Aging* **29**, 1404–1411 (2008).
3. Benjamini, Y. & Hochberg, Y. Controlling the false discovery rate: a practical and powerful approach to multiple testing. *J. R. Stat. Soc. B* **57**, 289–300 (1995).